ESTIMATION OF FLOODED AREAS DUE TO SUPERCYCLONE USING RADARSAT-1 SAR DATA AND DISCRIMINANT APPROACH-AN INDIAN CASE STUDY

[1]Abhijat A. Abhyankar, [2]Anand Patwardhan, and [3]Arun B. Inamdar
[1]Assistant Professor, National Institute of Construction Management and Research, Pune, India-aabhyankar@nicmar.ac.in
[2]Professor, Shailesh J. Mehta School of Management, IIT Bombay, Mumbai, India-anand@som.iitb.ac.in
[3]Associate Professor, Centre of Studies in Resources Engineering, IIT Bombay, Mumbai, India-abi@csre.iitb.ac.in

KEY WORDS: Radarsat-1 SAR, flooded areas, Fischer Discriminant Classification function

Abstract: The study aims to estimate flooded areas due to supercyclone using SAR data and discriminant analysis. We have considered the Orissa super cyclone as a case study that crossed the Orissa coast, India on October 30-31, 1999. The Kendrapara district of Orissa state was one of the affected districts due to this supercyclone and is considered as a study area.

For estimation of water and flooded areas, pre and post event Radarsat-1 SAR satellite images of October 11, 1999, November 2, 1999 and November 4, 1999 were analyzed. Field trip to the affected district was carried out after the super cyclone to get information on landcover classes (water and non water).

We applied the Fischer linear discriminant function to identify the threshold to classify water and non-water areas in pre event Radarsat-1 SAR image of October 11, 1999. We further determined water and submerged areas due to supercyclone in pre and post event Radarsat-1 SAR images. High overall accuracy results were obtained for the testing set data of October 11, 1999 Radarsat-1 SAR data.

INTRODUCTION

The Indian subcontinent faces by number of natural hazards namely, Tropical cyclones, Landslides, Earthquakes, Floods, Heat waves *etc.* The most frequent among them are cyclones. The damage and socioeconomic impact due to tropical cyclones is enormous. The damages are caused by strong winds, storm surges and heavy rainfall. Cyclone causes loss of life and property, inundation of low lying areas of coastal regions, erosion of beaches, embankments and reduction in soil fertility. Coastal inundation pollutes the drinking water sources causing outbreak of epidemics (http://www.imdmumbai.gov.in/scripts/detail.asp?releaseId=E0000CY4).

Remote sensing satellites have inherent advantages like extensive ground coverage, satellite revisit capability, and accessibility to the remotest parts. The satellites with optical sensors have been extensively used in natural resource management (*e.g.* Landsat, SPOT, Quickbird, Ikonos, IRS satellites *etc.*) and national development applications. These satellites applicability is reduced during floods/cyclones due to cloud cover. The satellites with microwave sensors have inherent cloud penetration capability and also distinctive water response. These have become a valuable tool for monitoring floods. Initially, Seasat and Shuttle Imaging Radar (SIR) showed the SAR data applicability in monitoring floods. Later new SAR satellites were launched namely, Radarsat-1/2, Envisat, JERS, ERS-1/2 *etc.* for various other applications *e.g.* geological, environmental *etc.*

Radar has inherent cloud penetration capability and distinctive water response and has become a valuable tool for monitoring floods. In the initial period itself, Seasat and Shuttle Imaging Radar (SIR) showed the SAR data applicability in monitoring floods (Ormbsy *et al.,* 1985). Later during the past two decades, various SAR satellites were launched namely, Radarsat-1/2 (Schumann, 2007), Envisat ASAR (Jiren, 2005), JERS (Yamada, 2002), ERS-1/2 (Badji and Dautrebande, 1997; Profeti and Macintosh, 1997) which were used in flood monitoring.

In SAR, the calm water shows least backscattering values among the natural objects in Microwave region. Also calm water and completely submerged landcovers under water have the same backscattering range (Lee *et al*, 2003; Shao *et al*, 2001). An attempt was made to map the flooded areas by Discriminant and Radarsat-1 SAR HH polarized data (Malnes *et al*, 2006). The flooded areas were estimated using Radarsat-1 SAR and deterministic approach for the Orissa supercyclone of 1999 (Abhyankar *et al*, 2006). Ogni storm crossed Andhra Pradesh on October 30, 2006. Satellite images (pre and post satellite images) of Envisat ASAR VV data and discriminant approach was used to identify flooded areas in few mandals of Guntur district (Abhyankar *et al*, 2011). It was found that a deterministic approach leads to overestimation or underestimation of flooded areas in the post event SAR images. In the present study, the authors attempt to identify water and flooded areas using the Envisat ASAR VV polarized data and discriminant approach.

STUDY AREA

This cyclone affected two states of India namely, West Bengal and Orissa. The Orissa supercyclone affected 12 districts of Orissa state. The affected districts in Orissa state due to this cyclone are given in Figure 1 and the selected district (*i.e.* Kendrapara district) for damage assessment due to Orissa supercyclone is given in Figure 2. The cyclone crossed the Orissa coastline on October 30-31, 1999. The strong winds, heavy rainfall and storm surge damaged crops, forests, and destroyed houses. This study focuses on one of the affected districts within Orissa state-Kendrapara (lying between Latitude 20°21' to 20°47'N and Longitude 86°14' to 87°83'E) with an area of 2644 sq kms. (District Statistical Handbook, Kendrapara, 2005). District is an administrative entity. The logic of taking a district as a unit of analysis is that the disaster management and administrative machinery is structured this way.

Due to this cyclone, 9781 people died and nearly 10 million people were affected. Also, communication network failed after the cyclone. A field visit to Kendrapara district of Orissa was carried after this supercyclone. During this visit the researcher recorded the latitude, longitude and the corresponding landcover class for a few locations. These was performed using hand held GPS. These sampled locations of the field were located on the pre event Radarsat-1 SAR image of October 11, 1999. We reduced the geometric errors (locational error) and different projections (GPS: WGS 84 and SOI toposheet: Everest) by extracting backscattering values from a 3 by 3 or 5 by 5 window.

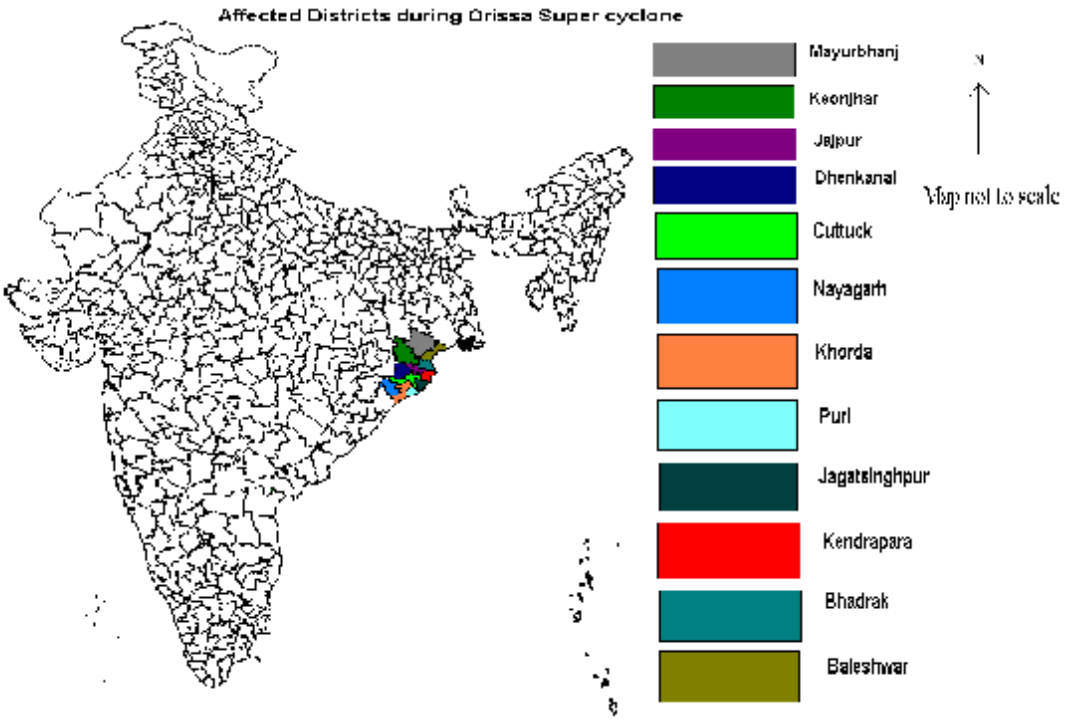

Figure 1: The affected districts of Orissa state during Orissa supercyclone

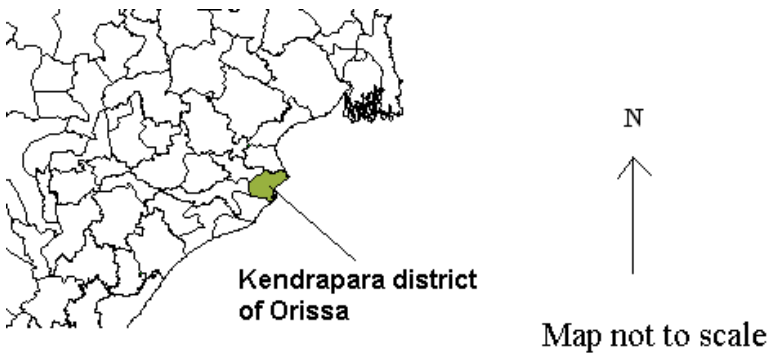

Figure 2: Kendrapara district-for assessment of flooded areas due to Orissa supercyclone

SATELLITE DATA

The pre processing analysis *viz.* speckle noise removal, data calibration and incidence angle correction were performed on Radarsat-1 SAR images.

Speckle noise in Radarsat-1 SAR imagery was reduced using Enhanced Lee Adaptive filter (Zhenghao and Fung, 1994). This filter performs spatial filtering on each individual pixel in an image using the grey-level values in a square window surrounding each pixel. In this study, a 5x5 average window was considered for smoothing. The resultant grey level value (R) for the smoothed pixel is:

$$\begin{aligned} R &= I_m && \text{for } C_i \text{ less than or equal to } C_u \\ R &= I_m \times W + I_c \times (1-W) && \text{for } C_u < C_i < C_{max} \\ R &= I_c && \text{for } C_i \text{ greater than or equal to } C_{max} \end{aligned} \quad (1)$$

Where,

I_m =Mean value of intensity within window;
I_c=Center pixel in filter window;
C_u=sqrt(1/NLook);
C_i=S/I_m; S=Standard deviation of intensity within window
C_{max}=sqrt (1+2/Nlook);
W=exp (-DF (C_i-C_u)/(C_{max}-C_i);
W=Weighting function;
NLOOK=Number of looks, value=1;
DF=Damping Factor, value=1

The data calibration and incidence angle correction exercise steps were performed (Chakraborty and Panigrahy, 2000). The incidence angle for each pixel i in a scanline is computed as given below:

$$I_i = \cos^{-1}[(H \times H - Rs_i \times Rs_i + 2 \times R \times H)/(2 \times Rs_i \times R)] \quad (2)$$

Where,

I_i=Incidence angle at the i^{th} range pixel;
Rs_i=Slant range;
H=Orbit altitude;
R=Radius of the earth.

It was found that the incidence angle range (in degrees) for the full image of October 11, 1999 was 30.1-46.5 whereas for November 2, 1999 and November 4, 1999 imageries the range was 19.3-38.9 and 19.0-47.0 respectively. Here, the area covered by a pixel is implicitly assumed to be horizontal in orientation. *e.g.* in agricultural areas the assumption is quite appropriate. Using this computed incidence angle, the backscattering coefficient σ_{0j} for the *j*th pixel in a scanline is computed as follows:

$$\sigma_{0j} = 10*\log_{10}[(DN_j^2 + A_0)/A_j] + 10*\log_{10}[\sin(I_j)] \text{(in dB)} \quad (3)$$

Where,

DN_j=Digital Number at the j^{th} range pixel;
A_j=Scaling gain value;
I_j=Incidence angle at the j^{th} range pixel;
A_0=Fixed gain offset, usually zero.

All the values are now obtained in dB *i.e.* backscattering values. The incidence angle range for the preprocessed images of October 11, 1999, November 2, 1999 and November 4, 1999 imageries was found to be 30.7 to 34.9, 32.6 to 37.6 and 20.4 to 27.3 respectively. Further, the Kendrapara district area was extracted from preprocessed full Radarsat-1 SAR images of October 11, 1999, November 2, 1999 and November 4, 1999 using standard digitized vector layer and the output is shown in Figure 3, Figure 4 and Figure 5 respectively. The data analysis was performed using ERDAS Imagine version 9.3 and PCI Geomatica version 8.2.3.

Visual analysis clearly shows qualitative changes in pre and post event images of study area (looking at Figure 3 and comparing with Figure 4 and Figure 5). These changes are due to Orissa supercyclone. Now it is important to determine quantitatively the changes due to this super cyclone and further assess the damage using these images.

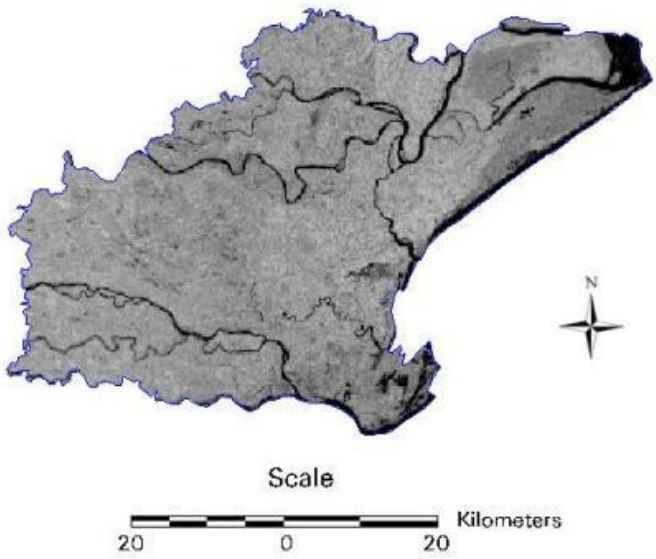

Figure 3: Pre event Radarsat-1 SAR image of October 11, 1999

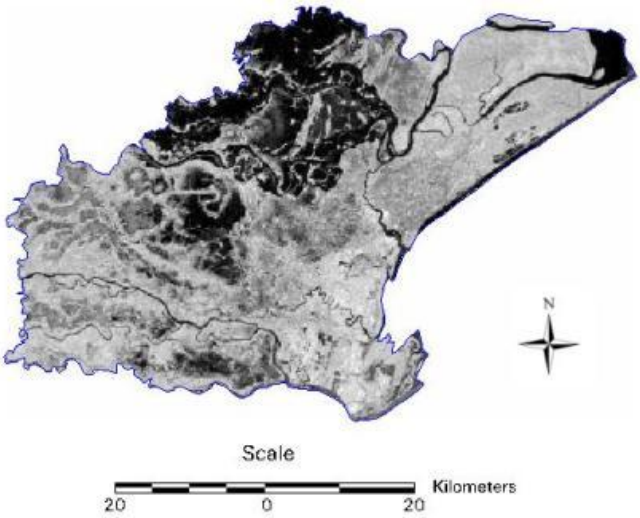

Figure 4: Post event Radarsat-1 SAR image of November 2, 1999

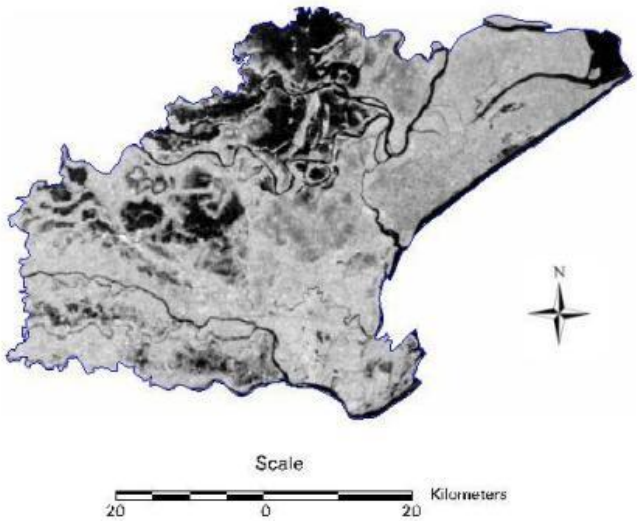

Figure 5: Post event Radarsat-1 SAR image of November 4, 1999

DATA ANALYSIS

The researcher collected information about landcover class of 666 pixels for pre event Radarasat-1 SAR image of October 11, 1999. This information about pixels and its landcover class (water and non water) was used for estimation or training and validation or testing of the models. Out of the total of 666 pixels, we selected randomly 486 pixels for estimation or training exercise (water=120 and non-water=366). For validation or testing exercise, the remaining 180 pixels were used (water=45 and non-water=135) *i.e.* 70% pixels in each class were considered for estimation or training of each class and remaining 30% were used for validation or testing (Paliwal and Kumar, 2009). The plot of training water and non-water pixels is shown in Figure 6. It can be seen from Figure 6 that there exists an overlap of backscattering values of water and non-water.

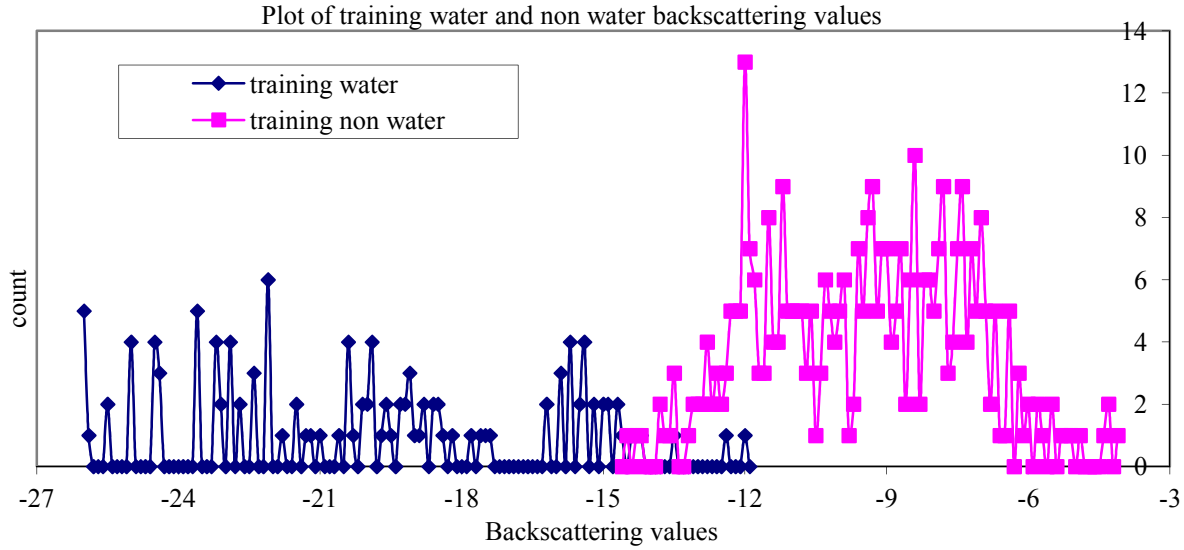

Figure 6: Plot of training water and non-water pixels

The descriptive statistics of training water and non-water pixels of October 11, 1999 Radarsat-1 SAR image is given in Table 1. The training water backscattering range is from -26.0 dB to -12.0 dB and non-water backscattering values range from -14.5 dB to -4.1 dB. If we select a threshold of -12.0 dB, then 59 pixels of non-water will get classified as water whereas if a threshold of -14.5 dB, six pixels of water will be classified as non-water. The extreme selection of threshold leads to overestimation or underestimation of landcover classes *i.e.* water or non-water. A threshold of -12.0 dB will lead to overestimation of water area and underestimation of non-water area and threshold of -14.5 dB will lead to underestimation of water area and over estimation of non-water area. A total of 65 pixels are in overlap region (*i.e.* -14.5 to -12.0 dB).

Table 1: Descriptive statistics of training water and non-water pixels

Parameters/Classes	Training water	Training non-water
Mean	-20.0	-9.5
Median	-20.0	-9.4
Mode	-22.1	-11.5
Standard Deviation	3.6	2.1
Kurtosis	-1.0	-0.7
Skewness	0.2	0.0
Range	14.0	10.3
Minimum	-26.0	-14.5
Maximum	-12.0	-4.1
Count	120.0	366.0

To avoid overestimation or underestimation of either classes (water or non-water), the discriminant method constructs a set of linear functions of the predictors. A threshold was identified by developing linear combination of training water and non-water *i.e.* we try to minimize the overestimation and under-estimation of both water and non-water class.

RESULTS AND DISCUSSION

Using Fisher's discriminant classification function, a threshold of -14.8 dB was identified to classify water and non-water in pre event image of October 11, 1999. At threshold of -14.8 dB, water area was underestimated by 7.5% and non-water underestimated by zero percent. At threshold of -14.8 dB, water area in Radarsat-1 satellite image of October 11, 1999 was found to be 20.646 thousand hectares. The same threshold was used for post event Radarsat-1 SAR images of November 2, 1999 and November 4, 1999 to identify completely submerged or partial/non submerged areas as water and completely submerged landcovers under water have same backscattering range. The water and completely submerged areas in November 2, 1999 and November 4, 1999 satellite images was found to be 68.8905 and 48.6097 thousand hectares respectively. The spatial distribution of water in pre event Radarsat-1 SAR is given in Figure 7. The spatial distribution of water and completely submerged landcovers in post event SAR images is given in Figure 8 and Figure 9.

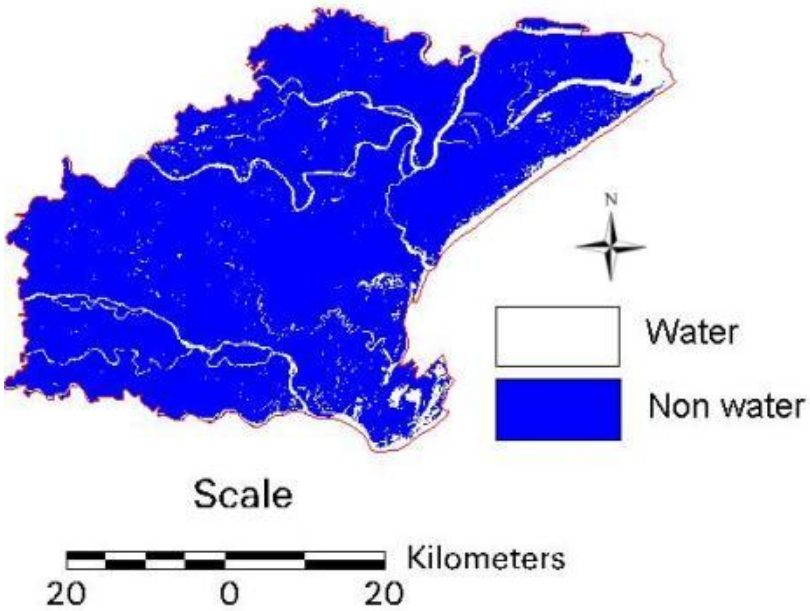

Figure7: Spatial distribution of water on October 11, 1999

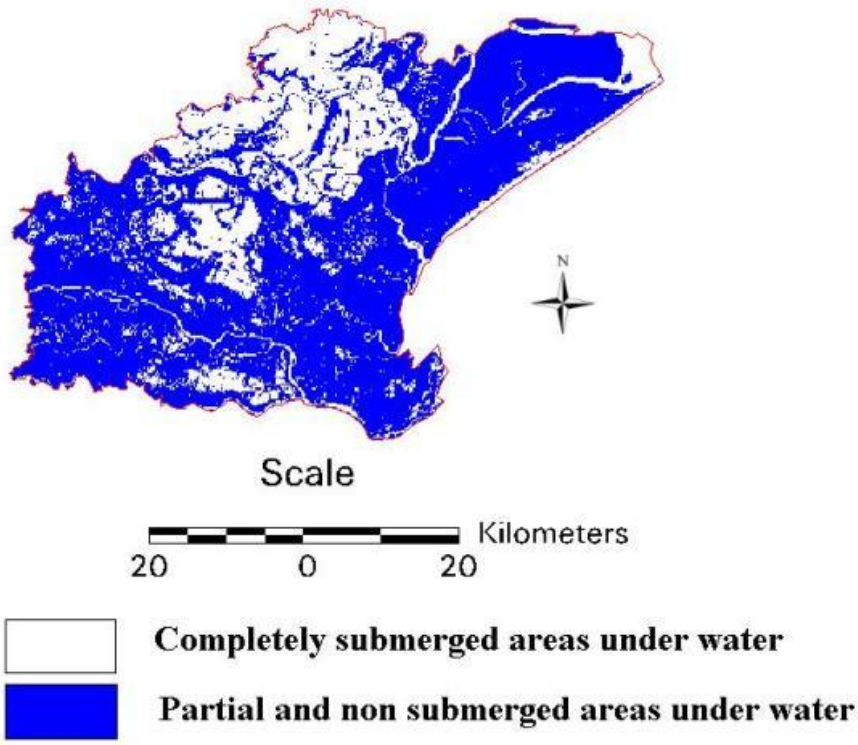

Figure 8: Spatial distribution of water and completely submerged areas on November 2, 1999

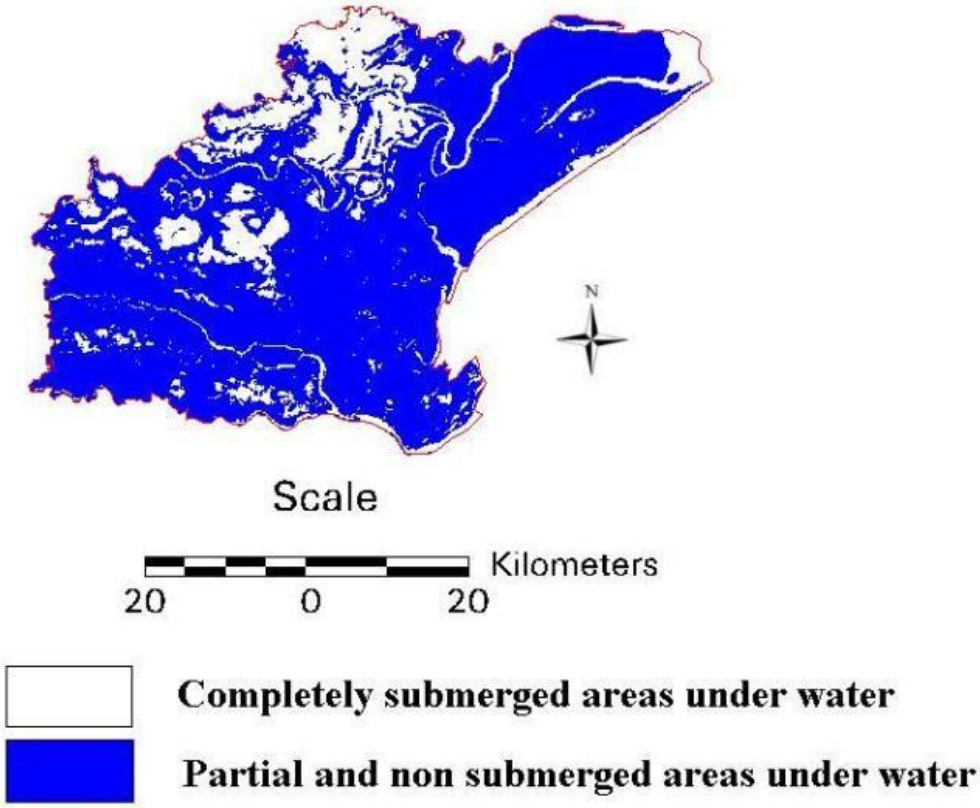

Figure 9: Spatial distribution of water and completely submerged areas on November 4, 1999

The confusion matrix for water and non-water was developed for the training dataset of October 11, 1999 (for the identified threshold of -14.8 dB to classify water and non-water) which is given in Table 2. Similarly, the confusion matrix for the test dataset was prepared and is given in Table 3.

Table 2: Confusion matrix for training set of October 11, 1999

Known / Classified	Water	Non water
Water	111	9
Non water	0	366

Overall accuracy=477/486=98.14%

Table 3: Confusion matrix for test set of October 11, 1999

Known / Classified	Water	Non water
Water	22	23
Non water	0	135

Overall accuracy=157/180=87.22%

CONCLUSION, LIMITATION AND FUTURE WORK

The flooded areas were extracted using Radarsat-1 SAR HH polarized data and Discriminant analysis. This technique reduces the overestimation or underestimation of water and flooded areas. In the present study, the water and non water training pixels are very small compared to the total pixels of study area.

Future work includes accurate estimation of paddy by SAR data. The accurate identification of paddy by SAR remains a challenge. The cyclonic incidences and paddy growing season overlap. Hence the present work can play a significant role in food security and relief measures. The cyclonic storms impact crops especially paddy (dominant crop in Indian coastal states/regions during cyclonic incidences) and reduce its productivity significantly. This directly leads to economic loss of the farmers. Therefore, it is of utmost importance to assess damage to paddy due to tropical cyclone. Also important is an appropriate release of proper monetary funds to the affected people and additional food grains to control food prices. The flood assessment methodology discussed above is rapid and accurate compared to survey techniques. Further fine tuning of methods involving satellite images will help in reducing the time frame for disaster monitoring and management.

REFERENCES

A. Abhyankar, A. Patwardhan, A. B. Inamdar (2006). Identification of Completely Submerged Areas due to Tropical Cyclone using Remotely Sensed Data: An Indian Case Study, IEEE International Geoscience and Remote Sensing Symposium, 3305-3308, July 31-August 4.

A. Abhyankar, A. Patwardhan, A. B. Inamdar (2011). Extraction of Flooded Areas due to Severe Storm using Envisat ASAR Data and Discriminant Approach, Geomatrix'11, the 2nd national conference on geospatial technologies and applications, February 26-27, IIT Bombay.

M.Chakraborty and S. Panigrahy (2000). A processing and software system for rice crop inventory using multi-date Radarsat ScanSAR data, *ISPRS Journal of Photogrammetry and Remote Sensing*, 55, 119-128.

M. Badji, and S. Dautrebande (1997). Characterization of flood inundated areas and delineation of poor drainage soil using ERS-1 SAR imagery, *Hydrological Processes*, 11(10), 1441-1450.

District Statistical Handbook, Kendrapara, 2005, Directorate of Economics and Statistics, Orissa, Bhubaneswar

E. Malnes, T. Guneriussen, and K. A. Hogda (2002). Mapping of flood area by Radarsat in Vansjo, Norway http://projects.itek.norut.no/snowman/Publications/Malnes1_ISRSE_2002.pdf (last accessed on August 31, 2012).

http://www.imdmumbai.gov.in/scripts/detail.asp?releaseId=E0000CY4 (last accessed on August 31, 2012)

G. Profeti and H. Macintosh (1997). Flood management through Landsat TM and ERS SAR data: a case study, *Hydrological Processes*, 11(10), 1397-1408.

J. P. Ormbsy, J. P. Blanchard, and A. J. Blanchard (1985). Detection of lowland flooding using active microwave systems, *Photogrammetric Engineering and Remote Sensing*, 51, 317-328.

M. Paliwal and A. K. Kumar (2009). Neural Network and statistical Techniques: A Review of applications. Expert Systems with application, 36, 2-17.

G. Schumann, R. Hostache, C. Puech, L. Hoffmann, P. Matgen, F. Pappenberger and L. Pfister (2007). High-resolution 3-D flood information from Radar imagery for flood hazard management, *IEEE Transactions on Geoscience and Remote Sensing*, 45(6), 1715-1725.

L Jiren and H. Shifeng (2005). Application of ERS/ENVISAT to flood monitoring and assessment in China, IEEE International Geoscience and Remote Sensing Symposium, 8, 5674-5677.

Y. Yamada, T. Sakurai-Amano, and M. Takagi (2002). Detection of flood damaged areas in the entire Chao Phraya River Basin from JERS-1/SAR images with a help of spatial information, IEEE International Geoscience and Remote Sensing Symposium, 5, 2877-2879.

S Zhenghao and K. B. Fung (1994). A comparison of digital speckle filters, IEEE International Geoscience and Remote Sensing Symposium, 4, 2129-2133.

K. S. Lee and S. I. Lee (2003). Assessment of post-flooding conditions of rice fields with multi-temporal SAR data. International Journal of Remote Sensing, 24 (17), 3457-3465.

Y. Shao, X. Fan, H. Liu, J. Xiao, S.Ross, B. Brisco, R. Brown, and G. Saples, (2001). Rice Monitoring and production estimation using multitemporal Radarsat, Remote Sensing of Environment, 76, 310-325.